Approach for CM/DM Current Extraction and Crosstalk Analysis of Twisted-Wire Pairs with Random Non-uniform Twisting

Chao Huang [1], Yan Zhao [1*], Wei Yan [1,2], Yanxing Ji [1], Qiangqiang Liu [1], Shijin Li [1], and Yi Cao [1]

[1] School of Electrical & Automation Engineering
Nanjing Normal University, Nanjing 210046, China
1547796467@qq.com, *zhaoyang2@njnu.edu.cn, 61197@njnu.edu.cn, 397832514@qq.com, 1376684687@qq.com, lishijin@njnu.edu.cn, caoyi@njnu.edu.cn.

[2] Zhenjiang Institute for Innovation and Development
Nanjing Normal University, Zhenjiang 212004, China

Abstract ─ In this paper, a twisted-wire pairs (TWP) with random non-uniform twisting is established. It is divided into a complete pitch segment and a non-complete pitch segment by the ratio between the pitch and the length. The randomness of the actual TWP cable is accurately simulated by the following methods: 1) random combination of complete pitch segments; 2) random combination of non-complete pitch segments; 3) random combination between 1) and 2). Based on the TWP model, an equivalent multi-conductor transmission lines (MTLs) model can be obtained. The neural network algorithm is introduced to describe the complex relationship between the arbitrary position of the TWP and the per-unit-length (p.u.l) parameter matrix. In addition, the crosstalk and the common-mode (CM) and differential-mode (DM) noise under field-to-wire coupling are predicted. The numerical results show that crosstalk and CM/DM noise in TWP cable are susceptible to the twisted pitch at high frequencies. Compared with full-wave simulation, the accuracy of the proposed method is proved.

Index Terms ─ Crosstalk, common-mode (CM) and differential-mode (DM), field-to-wire coupling, neural network algorithm, random non-uniform twisting, twisted-wire pairs (TWP).

I. INTRODUCTION

Twisted-wire pairs (TWP) cable often used in the automotive and aerospace industries have good resistance to electromagnetic interference [1-3]. With the rise of current operating frequencies, predictions involving crosstalk and field-to-wire coupling noise are still a challenging issue. Therefore, the establishment of the TWP model (especially considering the non-uniformities that occur randomly in the TWP in actual wiring) is of primary importance in the follow-up research.

Taylor and Spadacini have studied the field-to-wire coupling model of TWP in reference planes [4-6] and free space [7, 8]. In [5], a worst case model was proposed to solve the CM/DM noise problem under field-to-wire coupling. In [9], the *Monte Carlo* (MC) algorithm was introduced to statistically represent the randomness of manually assembled cables. As well as the *Random Midpoint Displacement* (RMD) algorithm in [10, 11] and the *Random Displacement Spline Interpolation* (RDSI) method in [12], they are used to model the randomness of the cable. Due to the discontinuities between adjacent sections of wires generated by these methods, TWP cable cannot be accurately simulated.

In recent research, the *Cubic Hermite Interpolation Polynomial* was used to ensure the continuity of the traverse [13, 14]. The inhomogeneity of the per-unit-length (p.u.l) parameter matrix and the role of reflection from the ground plane in the radiation sensitivity (RS) are also studied. The complex relationship between the TWP position and the p.u.l parameter matrix has been proved in [15] to be described by a neural network. In our previous research [15-17] and [18], the crosstalk results of the cables were obtained using the BAS-BP (back propagation algorithm optimized by the beetle antennae search method) neural network. For the modeling of TWP non-uniformity, the complete pitch segments are considered in [6], but the non-uniformity largely comes from the combination of non-complete pitch segments. In this paper, the geometric model of TWP in the real world is accurately simulated by considering the combination between complete and incomplete pitch segments. Use the neural network algorithm to obtain the p.u.l parameter matrix at any position, and calculate the crosstalk and CM/DM noise

Submitted On: May 17, 2020
Accepted On: July 9, 2020

https://doi.org/10.47037/2020.ACES.J.351204

in the TWP cable by FDTD method [19, 20].

This paper is organized as follows. In Section II, a TWP geometric model with random non-uniform twisting and a circuit model of wire-to-wire coupling and field-to-wire coupling are established. In Section III, the p.u.l parameter matrix is obtained by a neural network algorithm, and the crosstalk and CM/DM noise are predicted using FDTD technology. The comparison verification of the full-wave simulation based on the moment of method (MoM) is given in Section IV, and the results of crosstalk (CM/DM noise) are analyzed. Conclusions are eventually drawn in Section V.

II. GENERATION OF MODEL

A. Geometric model of TWP with random non-uniform twisting

TWP with random non-uniform twisting is a non-uniform transmission line. The model of TWP used in this paper is shown in Fig. 1. Traditional uniform TWP cables have the same twisting pitch, but due to manufacturing errors, random non-uniform twisting as shown in Fig. 1 may occur. Figure 1 (a) shows the model under the combination of different complete pitch segments (a certain cable length s_i is an integer multiple of the corresponding pitch p_i there); the model under different combinations of non-complete pitch segments (a certain cable length s_i is a non-integer multiple of the corresponding pitch p_i there) is shown in Fig. 1 (b); Fig. 1 (c) shows the model under the combination of complete pitch segments and non-complete pitch segments. The actual TWP is highly likely to be the model in Fig. 1 (c).

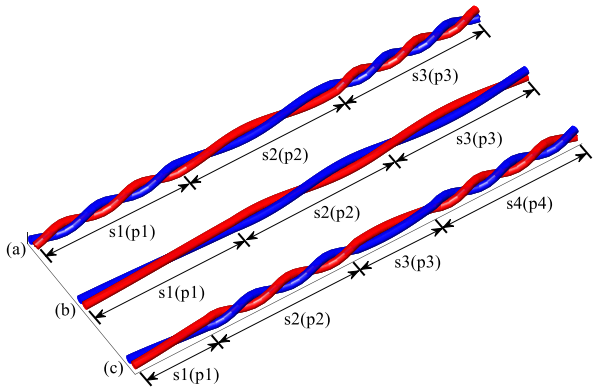

Fig. 1. TWP model with random non-uniform twisting. (a) TWP consisting of complete pitch segments. (b) TWP consisting of non-complete pitch segments. (c) TWP consisting of complete and non-complete pitch segments.

The wire is a cylindrical wire with an insulation layer, the wire radius is r, the center of the wire is d, the height of the twisted center from the ground is h, and the length of the TWP is L. The wire is twisted along the z-axis, and its parameters and reference ground are shown in Fig. 2 (b). The positions of the center points of the two wires are $\vec{l}_1$ and $\vec{l}_2$, which are expressed as follows:

$$\begin{cases} \vec{l}_1(x_1, y_1, z) = \frac{d}{2}\cos\theta\vec{a}_x + (h + \frac{d}{2}\sin\theta)\vec{a}_y + z\vec{a}_z \\ \vec{l}_2(x_2, y_2, z) = \frac{d}{2}\cos(\theta + \frac{\pi}{2})\vec{a}_x + (h + \frac{d}{2}\sin(\theta + \frac{\pi}{2}))\vec{a}_y + z\vec{a}_z \end{cases}, \quad (1)$$

where $\vec{a}_x$, $\vec{a}_y$, and $\vec{a}_z$ represent unit vectors of the x, y, and z axes, respectively. θ is the cross-section rotation angle at each position z, which is related to different pitch lengths:

$$\theta = f(z). \quad (2)$$

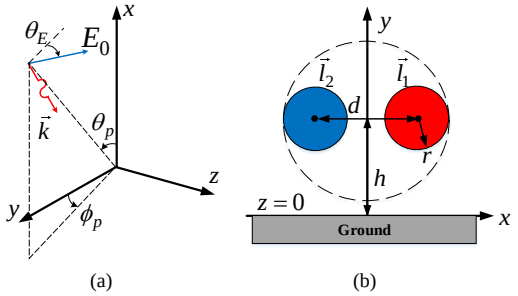

Fig. 2. External excitation field and cable parameters. (a) Plane wave electromagnetic field with electric field intensity E. (b) Cross section of initial position.

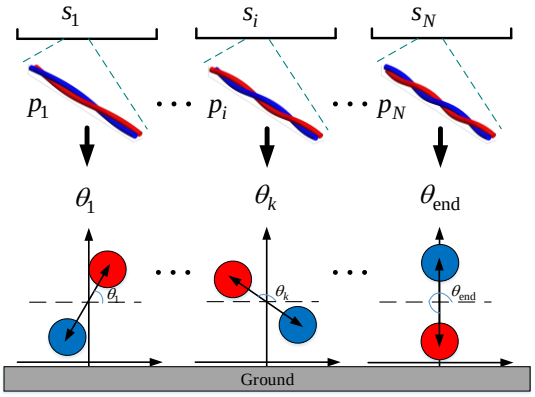

Fig. 3. Cross-section and rotation angle corresponding to different z values.

Figure 3 is a cross-section and a rotation angle at each z value obtained during the combination process based on Fig. 1 (c). S_i is the set of z values in a segment position in TWP, s_i is the length of the corresponding segment in the axial direction, and p_i is the type of the corresponding pitch length. The cross-section rotation angle in each section of S_i is:

$$\theta=\begin{cases}\dfrac{2\pi z}{p_1} & i=1, z\in S_1 \\ \displaystyle\sum_{j=1}^{i-1}\frac{2\pi s_j}{p_j}+\frac{2\pi(z-\sum_{j=1}^{i-1}s_j)}{p_i} & i\geq 2, z\in S_i\end{cases}. \tag{3}$$

The case of i=1 corresponds to uniform TWP, and the number of pitch types of general non-uniform TWP is all equal to or greater than two.

B. Circuit model with termination conditions

Large electromagnetic interference noise to TWP is mainly expressed by crosstalk in wire-to-wire coupling and CM/DM in field-to-wire coupling. Figures 4 (a) and (b) show the termination conditions in different situations. The equivalent circuit models of its unit length are shown in Figs. 4 (c) and (b). r_{ij}, l_{ij}, c_{ij}, and g_{ij} represent the elements in the parameter matrix of resistance **R**, inductance **L**, capacitance **C**, and conductance **G**, respectively, where i,j=1,2.

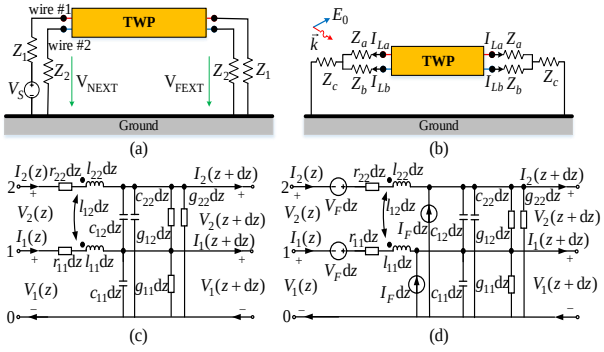

Fig. 4. Termination conditions and equivalent circuit. (a) Termination conditions for wire-to-wire coupling. (b) Termination conditions for field-to-wire coupling. (c) Unit equivalent circuit for wire-to-wire coupling. (d) Unit equivalent circuit for field-to-wire coupling.

The satisfied MTL equation [2] is:

$$\begin{cases}\dfrac{\partial \mathbf{V}(z,t)}{\partial z}+\mathbf{R}(z)\mathbf{I}(z,t)+\mathbf{L}(z)\dfrac{\partial \mathbf{I}(z,t)}{\partial t}=\mathbf{V}_F(z,t) \\ \dfrac{\partial \mathbf{I}(z,t)}{\partial z}+\mathbf{G}(z)\mathbf{V}(z,t)+\mathbf{C}(z)\dfrac{\partial \mathbf{V}(z,t)}{\partial t}=\mathbf{I}_F(z,t)\end{cases}, \tag{4}$$

where $\mathbf{V}(z,t)$, $\mathbf{I}(z,t)$ represent the voltage and current vectors of the cable at different positions z and at time t. $\mathbf{R}(z)$, $\mathbf{L}(z)$, $\mathbf{C}(z)$, and $\mathbf{G}(z)$ respectively represent the resistance, inductance, capacitance, and conductance matrix of the corresponding cross-sections at different positions z, that is, the per-unit-length (p.u.l) parameter matrix. $\mathbf{V}_F(z,t)$, $\mathbf{I}_F(z,t)$ represents the equivalent voltage and current sources of the external excitation field, which can be written as follows:

$$\begin{cases}\mathbf{V}_F(z,t)=\dfrac{\partial}{\partial z}\mathbf{E}_T(z,t)+\mathbf{E}_L(z,t) \\ \mathbf{I}_F(z,t)=\mathbf{C}(z)\dfrac{\partial}{\partial t}\mathbf{E}_T(z,t)\end{cases}, \tag{5}$$

where $\mathbf{E}_T(z,t)$ and $\mathbf{E}_L(z,t)$ represent the horizontal and vertical components of the incident electric field, respectively. Considering the non-uniformity of the TWP, z in each section of $\mathbf{E}_T$ and $\mathbf{E}_L$ can be approximately replaced by the z position at the left end.

The incident electric field is a uniform plane wave. The general expression is:

$$\vec{E}^{inc}(x,y,z,t)=(e_x\vec{a}_x+e_y\vec{a}_y+e_z\vec{a}_z)E_0(t-\frac{x}{v_x}-\frac{y}{v_y}-\frac{z}{v_z}). \tag{6}$$

The components of the incident electric field along the coordinate system are:

$$\begin{cases}e_x=\sin\theta_E\sin\theta_p \\ e_y=-\sin\theta_E\cos\theta_p\cos\phi_p-\cos\theta_E\sin\phi_p \\ e_z=-\sin\theta_E\cos\theta_p\sin\phi_p+\cos\theta_E\cos\phi_p\end{cases}, \tag{7}$$

where v_x, v_y, and v_z represent the components of the propagation velocity in each axis direction of the coordinate system:

$$\mathbf{E}_T(z,t)=\begin{bmatrix}\int_{x_0}^{x_1}E_x^{inc}(x_1,y_1,z,t)dx \\ \int_{x_0}^{x_2}E_x^{inc}(x_2,y_2,z,t)dx\end{bmatrix}, \tag{8}$$

$$\mathbf{E}_L(z,t)=\begin{bmatrix}E_z^{inc}(x_1,y_1,z,t)-E_z^{inc}(x_0,y_0,z,t) \\ E_z^{inc}(x_2,y_2,z,t)-E_z^{inc}(x_0,y_0,z,t)\end{bmatrix}, \tag{9}$$

where E_x^{inc} and E_z^{inc} are the horizontal and vertical components of the uniform plane wave. $E_z^{inc}(x_0,y_0,z,t)$ represents the magnitude of the longitudinal component at the reference ground (x_0=x, y_0=0).

As shown in Fig. 4 (a), the voltage and current on the transmission line also satisfy the formula (4) without applying an external excitation field. However, the equivalent voltage and current sources are set to zero, that is, $\mathbf{V_F}(z,t)$=$\mathbf{I_F}(z,t)$=**0**.

III. THE EXTRACTION AND APPLICATION OF P.U.L PARAMETER MATRIX

A. P.u.l parameter matrix

Equivalent voltage and current sources can be calculated using uniform plane waves. However, there are different p.u.l parameter matrices at different positions z. It is difficult to obtain a parameter matrix of any angle in the traditional way [14]. Any determined rotation angle of the cross-section has its own corresponding parameter matrix, and there is a non-

linear mapping relationship between the rotation angle and the parameter matrix. The transformations of the four p.u.l parameter matrices are the same. For simplicity, they can be expressed as follows:

$$\mathbf{M}(z)=\begin{bmatrix} m_{11} & m_{12} \\ m_{21} & m_{22} \end{bmatrix}, \tag{10}$$

where $\mathbf{M}(z)$ represents the cross-section $\mathbf{R}(z)$, $\mathbf{L}(z)$, $\mathbf{C}(z)$, $\mathbf{G}(z)$ p.u.l parameter matrix, and m_{ij} represents the specific resistance r_{ij}, inductance l_{ij}, capacitance c_{ij} and conductance g_{ij}. There is a complicated mathematical relationship between $\mathbf{M}(z)$ and the rotation angle:

$$\mathbf{M}(z) = g_{\mathbf{M}}(\theta). \tag{11}$$

In [17], the p.u.l parameter matrix corresponding to the different rotation angles of the cross-section can be obtained by prediction through the BAS-BP neural network. The network topology is shown in Fig. 5, but the hidden layer n_h and the output layer n_o are different from the previous [17].

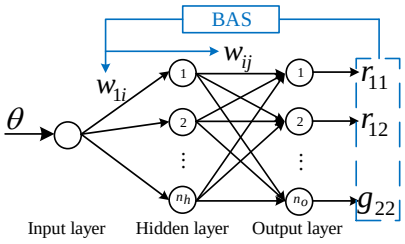

Fig. 5. Topological structure of BAS-BP neural network.

The input of the network is the cross-section rotation angle θ, and the output is a column vector consisting of the elements of the parameter matrix:

$$O=[r_{11}, r_{12}, r_{22}, l_{11}, l_{12}, l_{22}, c_{11}, c_{12}, c_{22}, g_{11}, g_{12}, g_{22}]^T. \tag{12}$$

After training the network with a small amount of data extracted in advance, the p.u.l parameter matrix of any rotation angle can be obtained. Considering the symmetry of the cross-section and the periodicity of the rotation angle, the input angle of the training network only needs 0°~180°. The result $\mathbf{M}(z')$ at 180°~360° only needs to perform row and column transformation on the corresponding prediction result $\mathbf{M}(z)$, as shown below. The result above 360° is the same as the corresponding result within 360°:

$$\mathbf{M}(z')=\begin{bmatrix} 0 & 1 \\ 1 & 0 \end{bmatrix}\mathbf{M}(z)\begin{bmatrix} 0 & 1 \\ 1 & 0 \end{bmatrix}. \tag{13}$$

B. Application in crosstalk

Considering the situation of Fig. 4 (c), the voltage and current are divided on the cable in space-time as shown in Fig. 6.

$\mathbf{V}_j^n$ and $\mathbf{I}_j^n$ in Fig. 6 can be expressed as:

$$\mathbf{V}_j^n = \mathbf{V}(j\Delta z, n\Delta t), \mathbf{I}_j^n = \mathbf{I}(j\Delta z, n\Delta t). \tag{14}$$

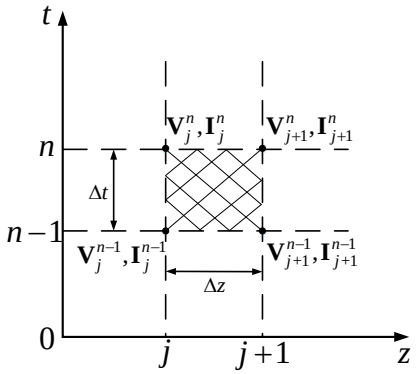

Fig. 6. Spatial-temporal dispersion of voltage and current.

Equation (4) can be discretized according to the Implicit-Wendroff format, as shown below:

$$\frac{\mathbf{V}_{j+1}^n - \mathbf{V}_j^n + \mathbf{V}_{j+1}^{n-1} - \mathbf{V}_j^{n-1}}{2\Delta z} + \frac{\mathbf{R}(j\Delta z)(\mathbf{I}_{j+1}^n + \mathbf{I}_j^n + \mathbf{I}_{j+1}^{n-1} + \mathbf{I}_j^{n-1})}{4} + \frac{\mathbf{L}(j\Delta z)(\mathbf{I}_j^n - \mathbf{I}_j^{n-1} + \mathbf{I}_{j+1}^n - \mathbf{I}_{j+1}^{n-1})}{2\Delta t} = 0, \tag{15}$$

$$\frac{\mathbf{I}_{j+1}^n - \mathbf{I}_j^n + \mathbf{I}_{j+1}^{n-1} - \mathbf{I}_j^{n-1}}{2\Delta z} + \frac{\mathbf{G}(j\Delta z)(\mathbf{V}_{j+1}^n + \mathbf{V}_j^n + \mathbf{V}_{j+1}^{n-1} + \mathbf{V}_j^{n-1})}{4} + \frac{\mathbf{C}(j\Delta z)(\mathbf{V}_j^n - \mathbf{V}_j^{n-1} + \mathbf{V}_{j+1}^n - \mathbf{V}_{j+1}^{n-1})}{2\Delta t} = 0. \tag{16}$$

Further simplified to:

$$\begin{cases} \mathbf{V}_j^n - \mathbf{V}_{j+1}^n + \mathbf{A}_{Vj}(\mathbf{I}_j^n + \mathbf{I}_{j+1}^n) = -\mathbf{V}_j^{n-1} + \mathbf{V}_{j+1}^{n-1} + \mathbf{B}_{Vj}(\mathbf{I}_j^{n-1} + \mathbf{I}_{j+1}^{n-1}) \\ \mathbf{A}_{Ij}(\mathbf{V}_j^n + \mathbf{V}_{j+1}^n) + \mathbf{I}_j^n - \mathbf{I}_{j+1}^n = \mathbf{B}_{Ij}(\mathbf{V}_j^{n-1} + \mathbf{V}_{j+1}^{n-1}) - \mathbf{I}_j^{n-1} + \mathbf{I}_{j+1}^{n-1} \end{cases}, \tag{17}$$

where the coefficient matrix is:

$$\begin{aligned} \mathbf{A}_{Vj} &= -(\mathbf{R}(j\Delta z)/2 + \mathbf{L}(j\Delta z)/\Delta t)\Delta z, \\ \mathbf{B}_{Vj} &= (\mathbf{R}(j\Delta z)/2 - \mathbf{L}(j\Delta z)/\Delta t)\Delta z, \end{aligned} \tag{18a}$$

$$\begin{aligned} \mathbf{A}_{Ij} &= -(\mathbf{G}(j\Delta z)/2 + \mathbf{C}(j\Delta z)/\Delta t)\Delta z, \\ \mathbf{B}_{Ij} &= (\mathbf{G}(j\Delta z)/2 - \mathbf{C}(j\Delta z)/\Delta t)\Delta z. \end{aligned} \tag{18b}$$

The termination load at both ends is Z_1=Z_2, and the excitation source Vs is added to one of the lines as the termination condition. Combining formulas (17), the near-end voltage $\mathbf{V}(0, t)$ and the far-end voltage $\mathbf{V}(L,t)$, and the voltage and current at any position and time can be obtained. Since the format (17) is unconditionally stable, the discrete solution of equation (17) converges to the analytical solution of equation (4). As for the near-end crosstalk (NEXT) and the far-end crosstalk (FEXT), the voltage can be transformed from the time domain to the frequency domain and is obtained by equation (19).

$$\mathrm{NEXT} = 20\log_{10}(V_2(0, f)/V_s), \tag{19a}$$

$$\mathrm{FEXT} = 20\log_{10}(V_2(L, f)/V_s). \tag{19b}$$

C. Application in CM/DM current under feld-to-wire coupling

Considering the situation of Fig. 4 (d) and the effect of a uniform plane wave, the same time-space division is shown in Fig. 6. The voltage and current satisfy equation (4), the difference is that it has the effect of uniform plane wave. The discretized equation is:

$$\mathbf{V}_j^n-\mathbf{V}_{j+1}^n+\mathbf{A}_{Vj}(\mathbf{I}_j^n+\mathbf{I}_{j+1}^n)=-\mathbf{V}_j^{n-1}+\mathbf{V}_{j+1}^{n-1}+\mathbf{E}_{Vj}+\mathbf{B}_{vj}(\mathbf{I}_j^{n-1}+\mathbf{I}_{j+1}^{n-1}), \tag{20}$$

$$\mathbf{A}_{Ij}(\mathbf{V}_j^n+\mathbf{V}_{j+1}^n)+\mathbf{I}_j^n-\mathbf{I}_{j+1}^n=-\mathbf{I}_j^{n-1}+\mathbf{I}_{j+1}^{n-1}+\mathbf{E}_{Ij}+\mathbf{B}_{Ij}(\mathbf{V}_j^{n-1}+\mathbf{V}_{j+1}^{n-1}), \tag{21}$$

where the other two parameter matrices are:

$$\begin{cases}\mathbf{E}_{Vj}=(\mathbf{A}_L-\dfrac{1}{v_z}\mathbf{A}_T)\dfrac{2\Delta z}{\Delta t}(E_0(n\Delta t-\dfrac{j\Delta z}{v_z})-E_0((n-1)\Delta t-\dfrac{j\Delta z}{v_z}))\\ \mathbf{E}_{Ij}=\mathbf{C}(j\Delta z)\mathbf{A}_T\dfrac{2\Delta z}{\Delta t}(E_0(n\Delta t-\dfrac{j\Delta z}{v_z})-E_0((n-1)\Delta t-\dfrac{j\Delta z}{v_z}))\end{cases}, \tag{22}$$

where

$$\mathbf{A}_T=\begin{bmatrix}e_x x_1+e_y y_1\\ e_x x_2+e_y y_2\end{bmatrix},\mathbf{A}_L=\begin{bmatrix}\dfrac{x_1}{v_x}+\dfrac{y_1}{v_y}\\ \dfrac{x_2}{v_x}+\dfrac{y_2}{v_y}\end{bmatrix}e_x. \tag{23}$$

The symmetrical load at both ends is Z_a=Z_b and Z_c, which constitutes the terminal condition. Combined with formula (21), the voltage and current at any position and time can be obtained. The CM/DM current at the left end of the circuit can be expressed as equation (24):

$$\mathrm{I}_{L-CM}=(I_1(0,f)+I_2(0,f))/2, \tag{24a}$$

$$\mathrm{I}_{L-DM}=(I_1(0,f)-I_2(0,f))/2. \tag{24b}$$

IV. NUMERICAL EXPERIMENT VERIFICATION AND ANALYSIS

A. Validation of the proposed method

The wire used in this paper is a copper core wire, and the outer insulation material is polyvinyl chloride (PVC). Where r=1.2mm, d=2r=2.4mm, h=8mm, L= 1m. The p.u.l parameter matrix set for network training is obtained by the finite element method (FEM) [16]. A set of data is extracted every 5° within 0°~180°, and a total of 36 sets of data are extracted for training network. The results are predicted using different random rotation angles and compared with the results obtained by FEM calculations. The relative errors of the pul parameter matrices **R**(z), **L**(z), **C**(z) and **G**(z) in the unit scales of Ω/m, nH/m, pF/m, and mS/m are shown in Fig. 7, which are all less than 5×10^{-3}.

In order to illustrate the accuracy of the proposed method in crosstalk prediction and CM/DM current prediction for TWP cable with random non-uniform twisting, a TWP model was randomly selected. The terminal port accesses the load, as shown in Fig. 4 (a) and Fig. 4 (b), respectively. Where Z_1=Z_2=50Ω, Z_a=Z_b=50Ω, Z_c=100Ω. As shown in Fig. 8, the prediction result under the wire-to-wire coupling and field-to-wire coupling (solid red line) are compared with the MoM (black dotted line) method. It can be seen from Table 1 that the maximum and minimum values of the average error are 3.524% and 0.158%, respectively.

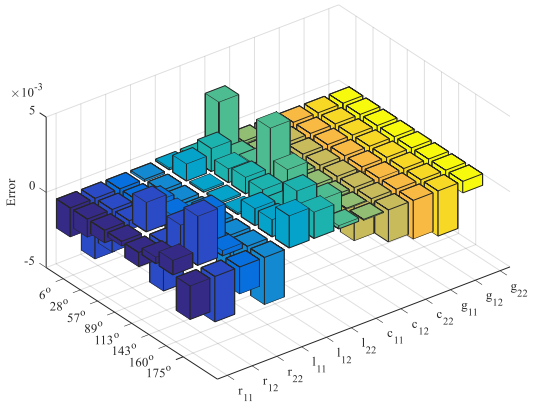

Fig. 7. Error histogram of p.u.l parameter matrix at different rotation angles.

The TWP cable is divided into 1000 sections. The externally applied excitation field is an uniform plane wave electric field incident at the port, where E_0=1V/m, θ_p=90°, ϕ_p=-90° and θ_E=90°. Considering the frequency of the signal source, the frequency range of the crosstalk result is 0.1MHz~1GHz, and the frequency range of the CM/DM current result is 1MHz~1GHz. The results further prove that the method in this paper has a more accurate prediction ability for the electromagnetic anti-interference performance of TWP cable with random non-uniform twisting.

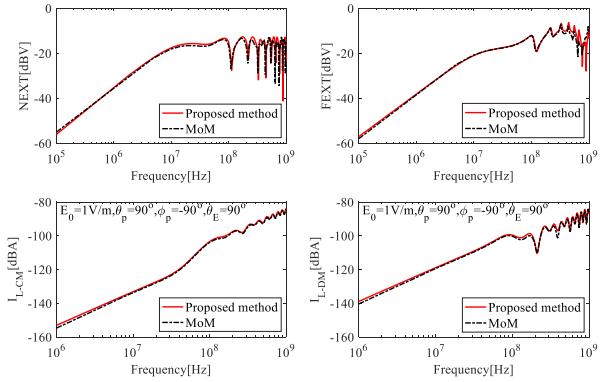

Fig. 8. Results verification of crosstalk and CM / DM current.

Table 1: Average error (%) of crosstalk and CM/DM current

Frequency (MHz)	0.1~100	100~500	500~1000
NEXT	2.140	1.864	1.131
FEXT	1.945	0.332	2.250
$I_{L\text{-}CM}$	3.524	0.158	0.948
$I_{L\text{-}DM}$	2.523	1.920	0.551

B. Prediction of crosstalk

The crosstalk results are shown in Fig. 9. Figures 9 (a) and 9 (b) are near-end crosstalk (NEXT) and far-end crosstalk (FEXT), respectively. A total of 500 sets of TWP models with random non-uniform twisting are calculated, and the CPU time of each set is 52.11s. NEXT and FEXT reach a minimum of -56.2dB and -57.3dB at 0.1MHz, respectively, and a maximum of -12.5dB and -6.23dB at 613MHz and 445MHz, respectively.

The ranges of the upper and lower envelope widths of the NEXT and NEXT curves are 0.024~25.197 dB and 0.045~17.483 dB, respectively. The envelope width fluctuates less in the low frequency range, indicating that different TWP models are less affected. The envelope width changes greatly in the high-frequency range, indicating that the TWP models is susceptible to high-frequency signals, and its crosstalk increases correspondingly.

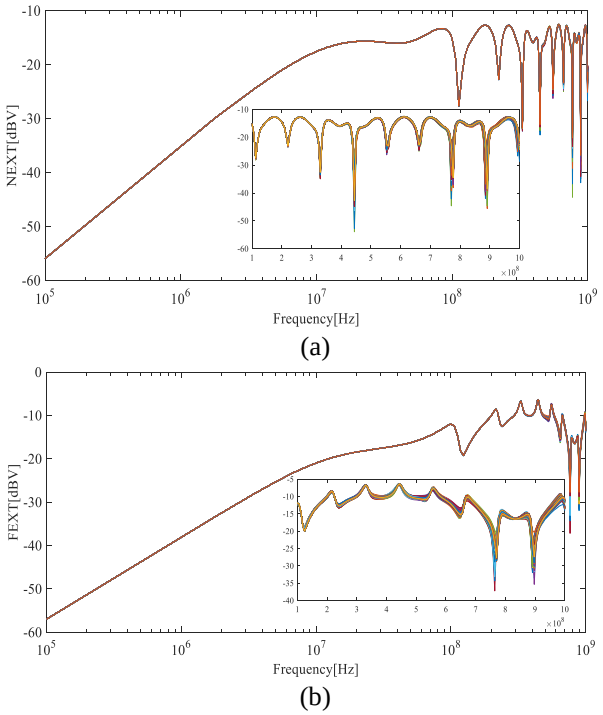

Fig. 9. Wire-to-wire coupling model: crosstalk prediction. (a) Near-end crosstalk (NEXT). (b) Far-end crosstalk (FEXT).

C. Prediction of CM/DM currents

The results of the CM and DM currents irradiated by the plane electric field wave incident at the port are shown in Fig. 10. Figures 10 (a) and 10 (b) show the CM current and DM current, respectively. As with crosstalk, 500 groups of the TWP models are calculated, and the CPU time of each group is 68.74s. The maximum and minimum of CM and DM currents are much reduced compared to crosstalk. This indicates that the effect of field-to-wire coupling is less than the effect of wire-to-wire coupling. The overall trend of CM and DM currents is a straight rise along a slope of 20dB/decade, and the amplitude fluctuation in the high frequency region is small.

The envelope widths of CM and DM currents are 0.399~2.369dB and 0.208~11.695dB, respectively. The envelope width of the CM current is more evenly distributed over the entire frequency range. The envelope width of the DM current is smaller in the low frequency range, but is larger in the high frequency range. This shows that the DM current of the TWP model is more susceptible to high frequency signals.

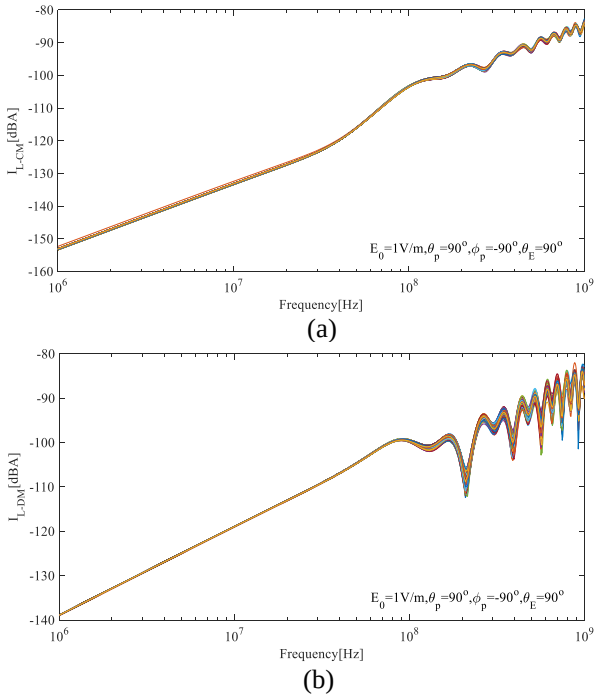

Fig. 10. Field-to-wire coupling model: CM and DM current prediction. (a) CM current and (b) DM current.

Figure 10 is a CM and DM current curve under the irradiation of a plane wave incident at a port. The general actual situation is that the position and the incident angle of the plane wave are both random irradiation with uncertainty. The field-to-wire coupling model under the random position uniform plane wave irradiation is shown in Fig. 11. Figures 11 (a) and 11 (b) show the CM

current and DM current, respectively. A total of 1,000 TWP models under uniform plane wave irradiation with random positions were calculated, and the CPU time spent by each group was 71.83s.

The envelope widths of CM and DM currents are 29.873~56.783dB and 29.755~56.823dB, respectively. Its width is larger than that of a single plane wave. Compared with Fig. 10, CM and DM are greatly affected by the externally applied excitation field. The reason is that the amplitudes of the CM and DM currents are mainly determined by the externally applied excitation field.

It can be seen that all the curves are under the black dotted line in Fig. 11, which represent the worst case of the CM and DM currents. Its initial values start from -143.31dB and -78.46dB, respectively. It can be noticed that the curve of Fig. 10 will show different changing trends in some frequency ranges. This is because different wave angles may cause the observed CM and DM currents to increase or decrease.

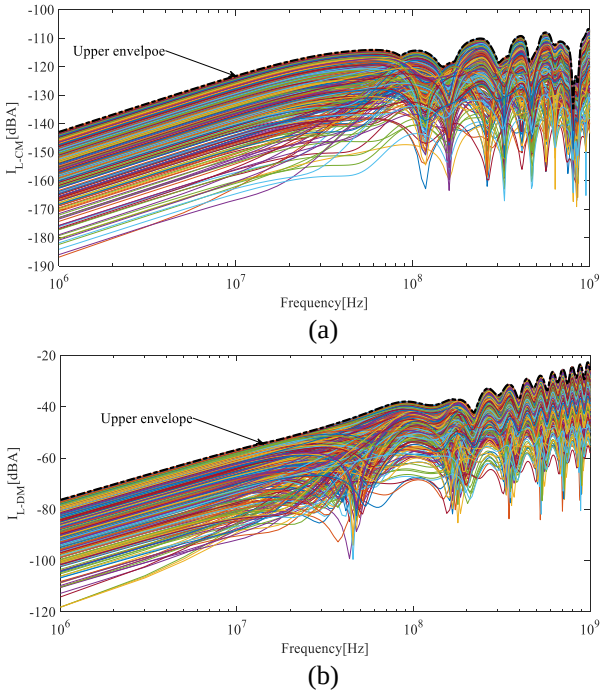

Fig. 11. Field-to-wire coupling model under uniform plane wave irradiation at random position. (a) CM current and (b) DM current.

V. CONCLUSION

In this paper, a new TWP model is proposed. The model considers the randomness of the twisting pitch and the combination of different pitch types. A TWP model is established for the combination of complete pitch segments and non-complete pitch segments, which overcomes the randomness problem in the references.

The p.u.l parameter matrix at any position was obtained by a neural network algorithm, and the FDTD method was used to solve the crosstalk under the wire-to-wire coupling model and the CM/DM current under the field-to-wire coupling model. The full-wave electromagnetic simulation (based on the MoM method) is used for comparison and verification, which proves that the proposed method has high accuracy.

In crosstalk results, TWP with random non-uniform twisting are susceptible to high-frequency signals, and the low-frequency range is less affected. In the CM and DM noise results, the DM current is more susceptible to high-frequency signals than the CM current. However, for CM and DM currents, the impact of uniform plane wave irradiation position and wave angle is greater than the effect of random non-uniform twist pitch. These influencing factors will have important reference significance in subsequent research and engineering applications.

ACKNOWLEDGMENT

The paper is supported by National Natural Science Foundation of China (51475246), National Natural Science Foundation of Jiangsu Province (BK20161019), Aviation Science Foundation (20172552017), and Nanjing International Industrial Technology R&D Cooperation Project under Grant 201911021.

REFERENCES

[1] F. Grassi, "Immunity to conducted noise of data transmission along DC power lines involving twisted-wire pairs above ground," *IEEE Trans. Electromagn. Compat.*, vol. 55, no. 1, pp. 195-207, Feb. 2013.

[2] C. R. Paul, *Analysis of Multiconductor Transmission Lines*. 2nd ed., New York, USA: Wiley, 1994.

[3] C. D. Taylor and J. P. Castillo, "On the response of a terminated twisted-wire cable excited by a plane-wave electromagnetic field," *IEEE Trans. Electromagn. Compat.*, vol. 22, no. 1, pp. 16-19, Feb. 1980.

[4] R. Stolle, "Electromagnetic coupling of twisted pair cables," *IEEE J. Sel. Areas Comm.*, vol. 20, no. 5, pp. 883-892, June 2002.

[5] G. Spadacini, F. Grassi, F. Marliani, and S. A. Pignari, "Transmission-line model for field-to-wire coupling in bundles of twisted-wire pairs above ground," *IEEE Trans. Electromagn. Compat.*, vol. 56, no. 6, pp. 1682-1690, Dec. 2014.

[6] G. Spadacini and S. A. Pignari, "Numerical assessment of radiated susceptibility of twisted-wire pairs with random non-uniform twisting," *IEEE Trans. Electromagn. Compat.*, vol. 55, no. 5, pp. 956-964, Jan. 2013.

[7] G. Spadacini and S. A. Pignari, "Radiated susceptibility of a twisted-wire pair illuminated by a random plane-wave spectrum," *IEICE Trans.*

Commun., vol. E93-B, no. 7, pp. 1781-1787, July 2010.

[8] S. A. Pignari and G. Spadacini, "Plane-wave coupling to a twisted-wire pair above ground," *IEEE Trans. Electromagn. Compat*., vol. 53, no. 2, pp. 508-523, May 2011.

[9] S. Shiran, B. Reiser, and H. Cory, "A probabilistic model for the evaluation of coupling between transmission lines," *IEEE Trans. Electromagn. Compat.*, vol. 35, no. 3, pp. 387-393, Aug. 1993.

[10] D. Weiner and G. Capraro, "A statistical approach to EMI theory and experiment - Part 2," *presented at the 1987 Zurich Symp. Electromagn. Compat*., Zurich, Switzerland, 1987.

[11] S. Salio, F. Canavero, D. Lecointe, and W. Tabbara, "Crosstalk prediction on wire bundles by Kriging approach," *in Proc. IEEE Int. Symp. Electromagn. Compat*., vol. 1, pp. 197-202, 2000.

[12] S. Sun, G. Liu, J. L. Drewniak, and D. J. Pommerenke, "Hand-assembled cable bundle modeling for crosstalk and common-mode radiation prediction," *IEEE Trans. Electromagn. Compat*., vol. 49, no. 3, pp. 708-718, Aug. 2007.

[13] A. Shoory, M. Rubinstein, A. Rubinstein, C. Romero, N. Mora, and F. Rachidi, "Application of the cascaded transmission line theory of Paul and McKnight to the evaluation of NEXT and FEXT in twisted wire pair bundles," *IEEE Trans. Electromagn. Compat*., vol. 55, no. 4, pp. 648-656, Aug. 2013.

[14] X. K. Liu, F. Grassi, G. Spadacini, and S. A. Pignari, "Physically based modeling of hand-assembled wire bundles for accurate EMC prediction," *IEEE Trans. Electromagn. Compat*., pp. 1-9, June 2019.

[15] C. P. Yang, W. Yan, Y. Zhao, Y. Chen, C. M. Zhu, and Z. B. Zhu, "Analysis on RLCG parameter matrix extraction for multi-core twisted cable based on back propagation neural network algorithm," *IEEE Access*., vol. 7, pp. 126315-126322, Aug. 2019.

[16] Y. Zhao and Y. Y. Wang, "A new finite-element solution for parameter extraction of multilayer and multiconductor interconnects," *IEEE Microwave and Guided Wave Letters.*, vol. 7, no. 6, pp. 156-158, June 1997.

[17] C. Huang, W. Yan, Y. Zhao, Q. Q. Liu, and J. M. Zhou, "A new method for predicting crosstalk of random cable bundle based on BAS-BP neural network algorithm," *IEEE Access*, vol. 8, pp. 20224-20232, Jan. 2020.

[18] F. Dai, G. H. Bao, and D. L. Su, "Crosstalk prediction in non-uniform cable bundles based on neural network," *Proceedings of the 9th International Symposium on Antennas, Propagation and EM Theory*, Guangzhou, pp. 1043-1046, 2010.

[19] A. T. Matsu, F. Rachidi, and M. Rubinstein, "A technique for calculating voltages induced on twisted-wire pairs using the FDTD method," *IEEE Trans. Electromagn. Compat*., vol. 59, no. 1, pp. 301-304, Oct. 2016.

[20] P. F. Zhang, X. L. Du, J. Zou, J. S. Yuan, and S. L. Huang, "Iterative solution of MTL based on the spatial decomposition and the second-order FDTD," *IEEE Trans. Magnetics*., vol. 54, no. 3, pp. 1185-1193, Mar. 2018.

Chao Huang was born in Anhui Province, China. He received the B.S degree in School of Electrical Engineering and Automation from Anhui University of Technology, Maanshan, China, in 2018. He is currently working toward the Master's degree in Electrical Engineering at Nanjing Normal University, Nanjing, China. His main research interests include multi-conductor transmission lines and EMC.

Yang Zhao received his B.E., M.E., and Ph.D. degree all in Power Electronic Technology from Nanjing University of Aeronautics and Astronautics, Nanjing, China, in 1989 and 1992, and 1995, respectively. He is currently the Professor with Nanjing Normal University. His research interests are in the areas of Electromagnetic Compatibility, Power Electronics and Automotive Electronics.

Wei Yan Doctor & Assoc. Professor from Nanjing Normal University. He obtained the Physics and Electronics Ph.D. and Electrical Engineering M.S. from Nanjing Normal University in 2014 and 2011. He is the Senior Member of China Electrical Technology Association and the evaluation expert of the Electromagnetic Compatibility Calibration Specification of China.